Contrasting photophsical properties of rhenium(I) tricarbonyl complexes having carbazole groups attached to the polypyridine ligand

Luiz D. Ramos, Renato N. Sampaio, Francisco F. de Assis, Kleber T. de Oliveira, Paula Homem-de-Mello, Antonio Otavio T. Patrocinio, Karina P.M. Frin

Supporting Information

Table S1: Structural and vibrational data of fac-[Re(L)(cbz$_2$phen)(CO)$_3$]$^{0/+}$ compounds.

| Bond Lenght	L		
	Cl$^-$	py	ampy
Re-C (equatorial) (Å)	1.91	1.92	1.92
Re-C (ancillary) (Å)	1.90	1.92	1.92
Re-N (Å)	2.15	2.16	2.16
Re-X (Å)	2.52	2.20	2.25
N-Re-N (°)	76.3	76.13	75.99

| Compounds	Calculated (cm^{-1}) mPW1PW91/LANL2DZ	Experimental (cm^{-1})
fac-[ReCl(CO)$_3$(cbz$_2$phen)]	2023.10; 1941.67; 1916.85	2020; 1916; 1895
fac-[Re(py)(CO)$_3$(cbz$_2$phen)]$^+$	2039.35; 1957.22; 1945.56	2030; 1923
fac-[Re(ampy)(CO)$_3$(cbz$_2$phen)]$^+$	2034.73; 1949.54; 1934.21	2025; 1901

Figure S1a: ^{1}H NMR spectrum of cbz$_2$phen (CDCl$_3$/500MHz, 25 °C).
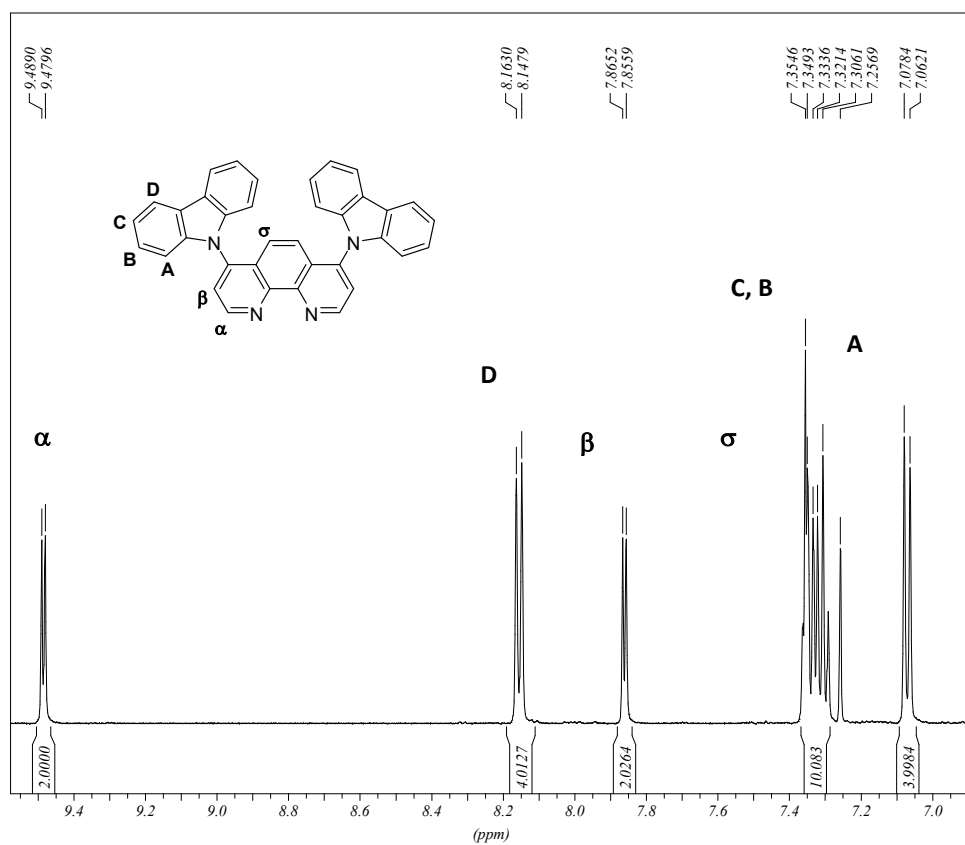
Figure S1b: ^{13}C{^{1}H} NMR spectrum of cbz$_2$phen (CDCl$_3$/125MHz, 25 °C).
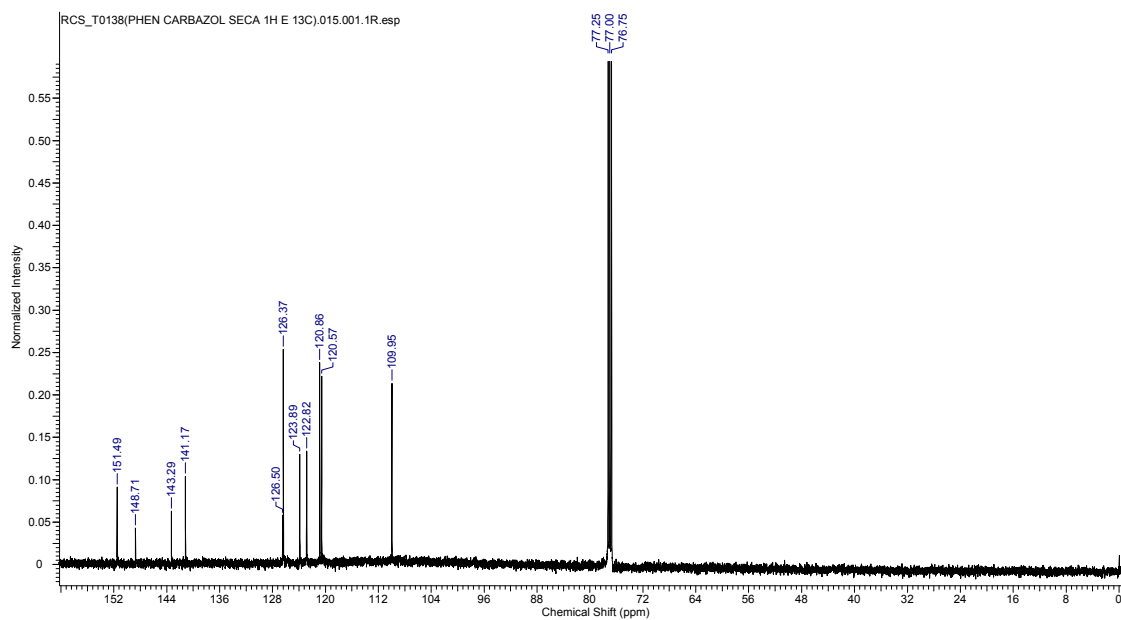
Figure S1c: DEPT-135 ^{13}C NMR spectrum of cbz$_2$phen (CDCl$_3$/125MHz, 25 °C)
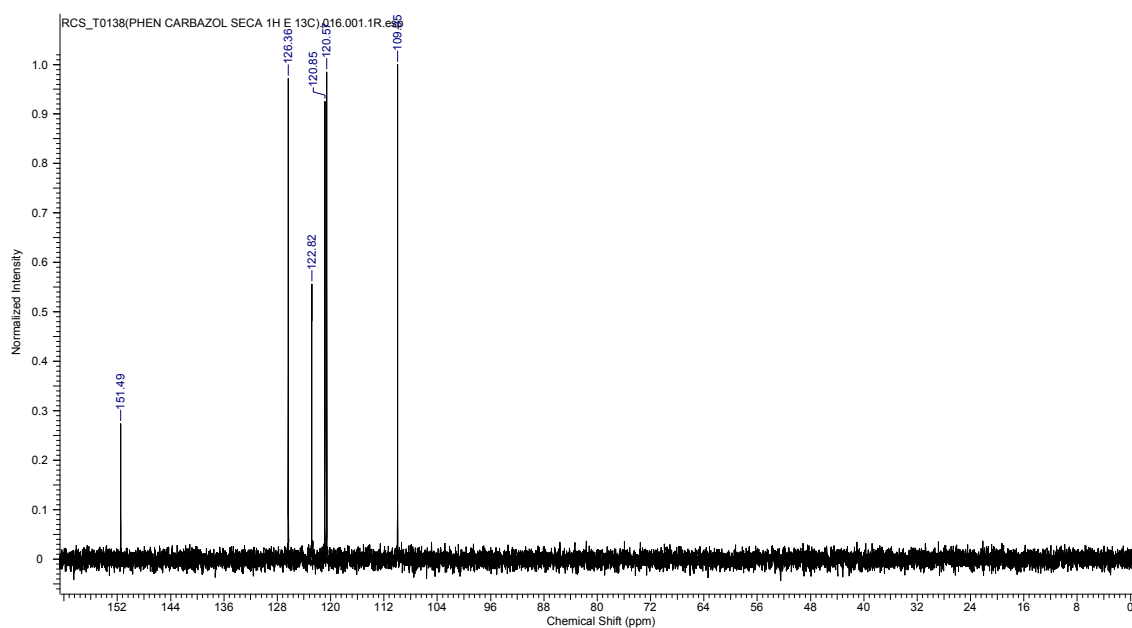
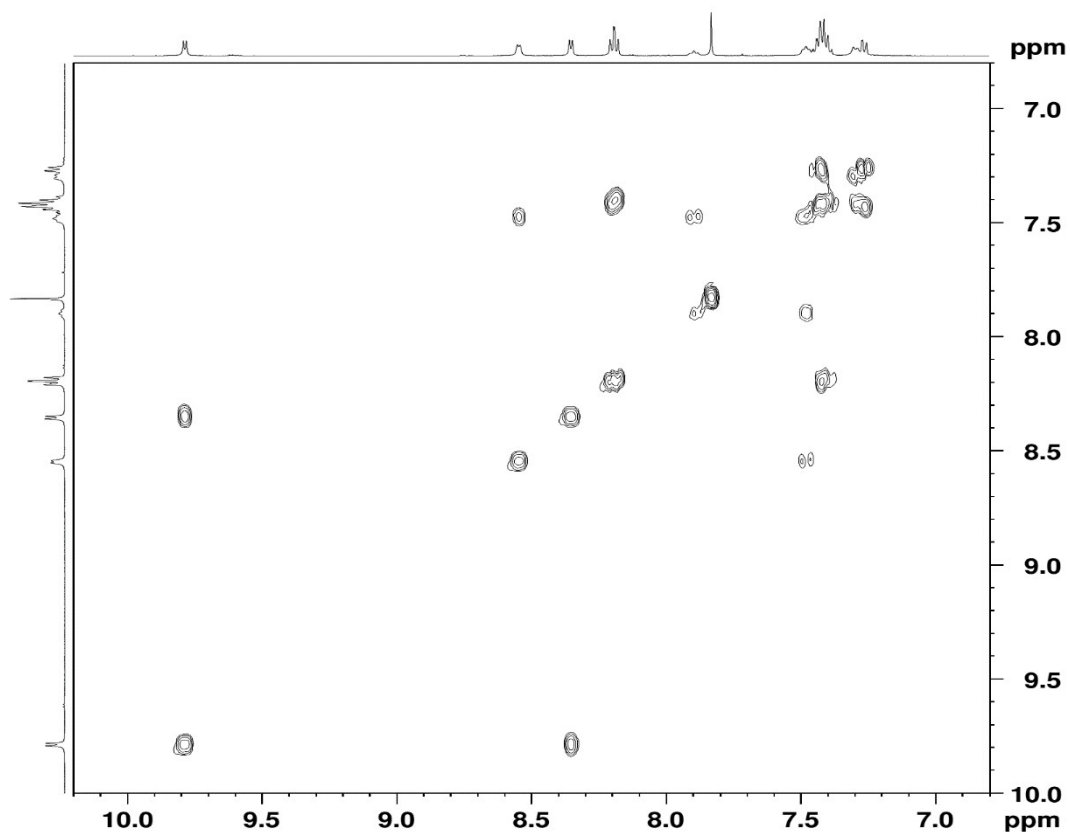**Figure S2**: ^{1}H NMR spectrum of *fac*-[ReCl(CO)$_3$(cbz$_2$phen)] (CD$_2$Cl$_2$/500MHz, 25 °C).
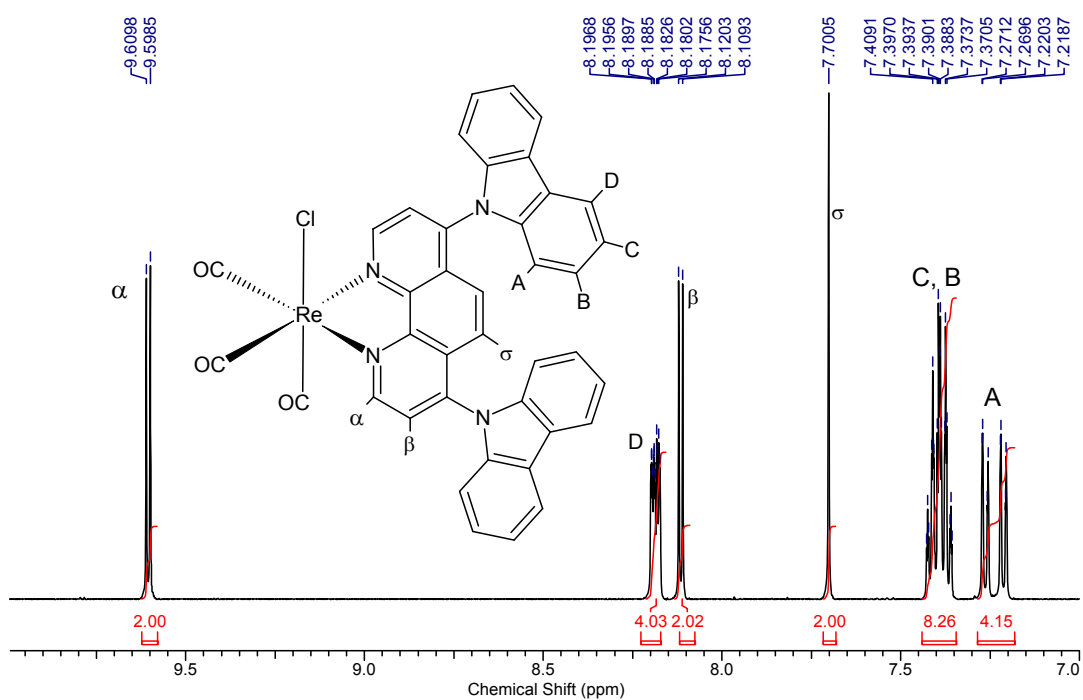
Figure S3: *H-H COSY* spectrum of *fac*-[ReCl(CO)₃(cbz₂phen)] (CD₂Cl₂/500MHz, 25 °C)
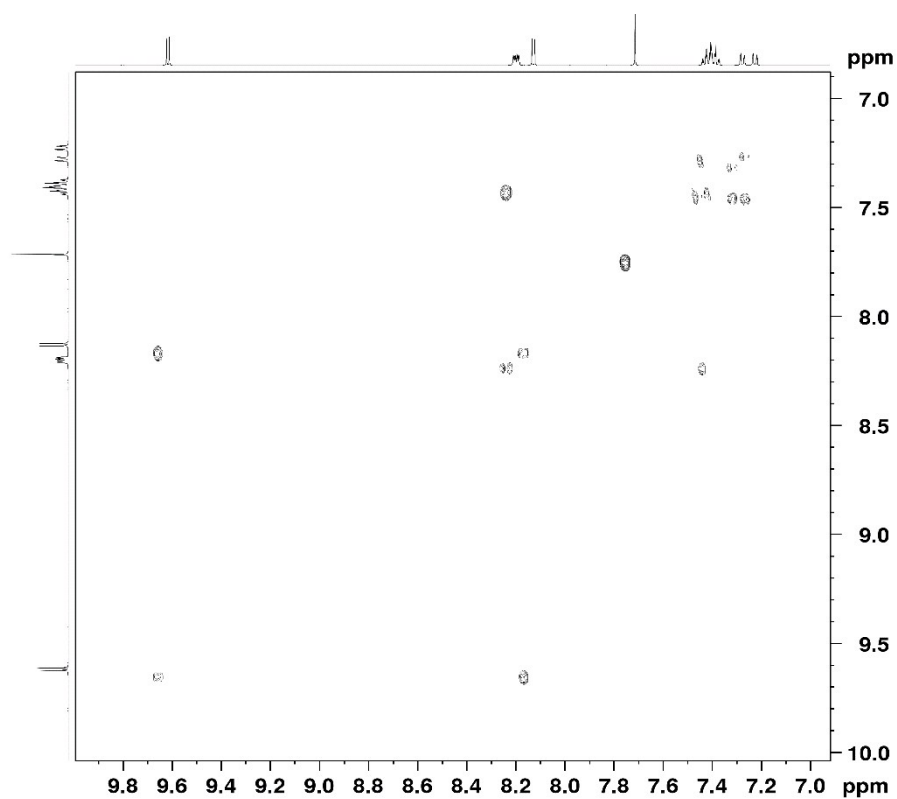
Figure S4: ¹H NMR spectrum of *fac*-[Re(CO)₃(cbz₂phen)(py)]⁺ (CD₂Cl₂/500MHz, 25 °C)
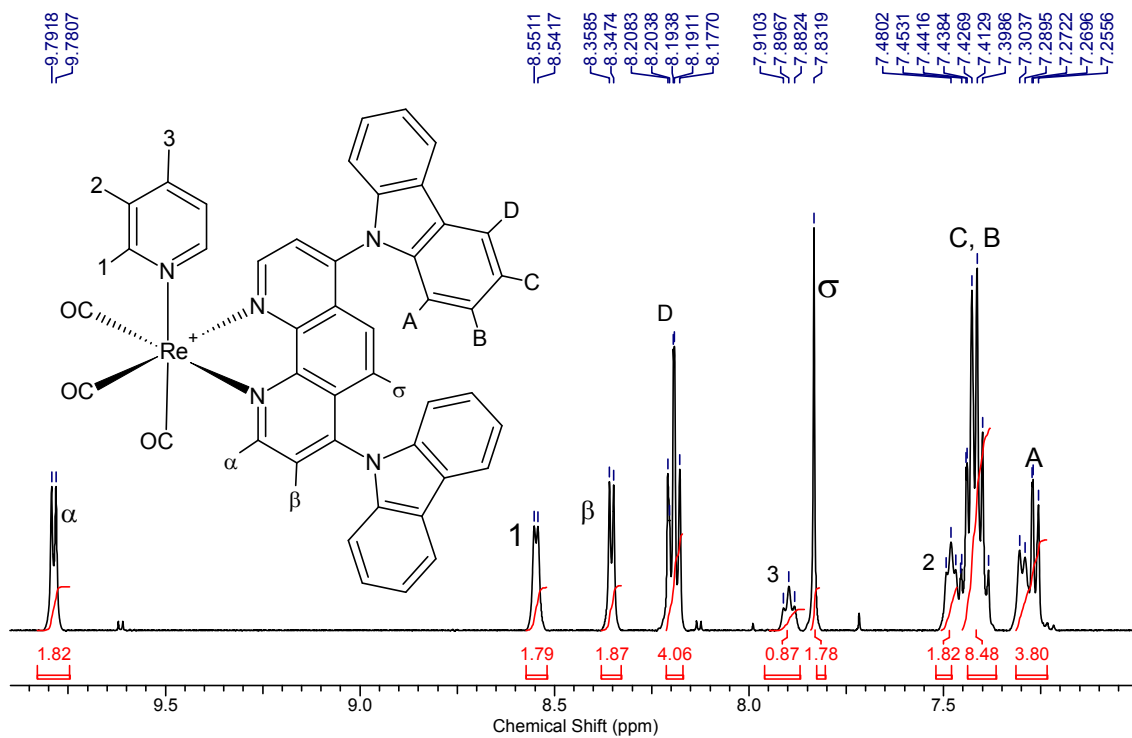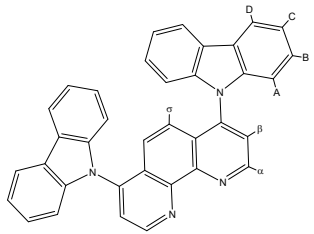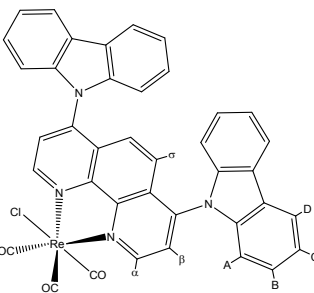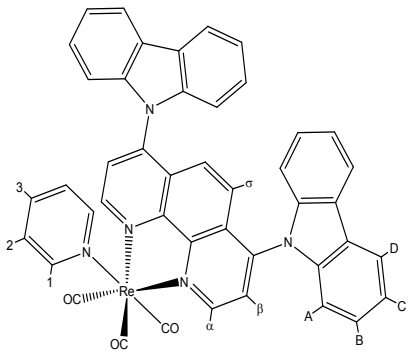
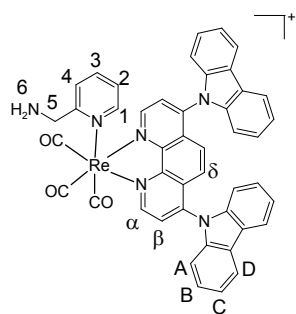**Figure S5:** *H-H COSY* spectrum of *fac*-[Re(py)(CO)$_3$(cbz$_2$phen)]+ (CD$_2$Cl$_2$/500 MHz, 25 °C)

Figure S6: ^{1}H NMR spectrum of *fac*-[Re(CO)$_3$(cbz$_2$phen)(ampy)]$^+$ (CD$_2$Cl$_2$/500 MHz, 25 °C)
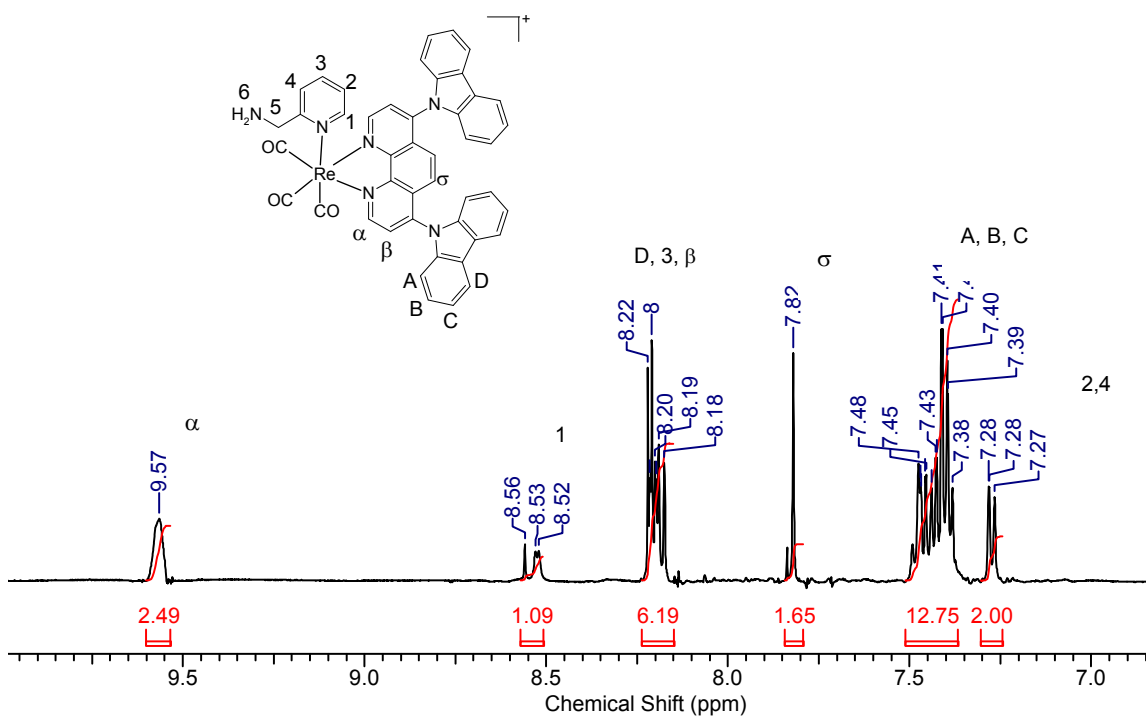
Table S2: ^{1}H NMR spectral data for rhenium(I) complexes and ligand.

Compound	Proton	δ(ppm)	J(Hz)
	Hα(d)	9.5	4.7
	Hβ(d)	7.9	4.7
	Hσ(s)	7.4	
	HB(m)	7.3	
	HA(d)	7.1	8.1
	HC(m)	7.3	
	HD(d)	8.1	7.6
	Hα (d)	9.6	5.6
	Hβ (d)	8.1	5.6
	Hσ (s)	7.7	
	HB (m)	7.4	
	HA(dd)	7.2	7.2
	HC (m)	7.4	
	HD (m)	8.2	
	Hα(d)	9.8	5.4
	Hβ(d)	8.4	5.4
	Hσ(s)	7.8	
	HB(m)	7.4	
	HA(dd)	7.3	6.9; 7.7
	HC(m)	7.4	
	HD(t)	8.2	8.1; 7.1
	H1(d)	8.5	4.4
	H2(d)	7.5	
	H3(t)	7.9	

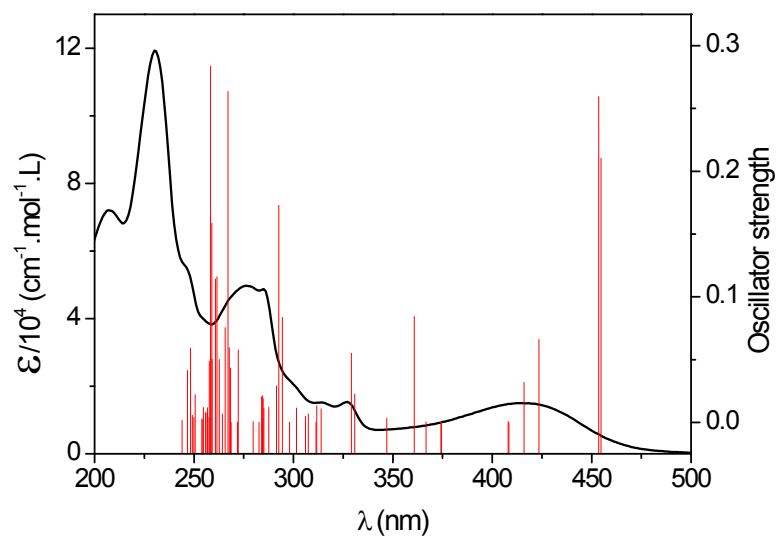|		
Hα(m)	9.6	
Hβ(m)	8.2	
Hσ(s)	7.8	
HB(m)	7.4	
HA(m)	7.4	
HC(m)	7.4	
HD(m)	8.2	
H1(d)	8.5	5.0
H2(d)	7.3	5.0
H3(m)	8.2	
H4(d)	7.3	5.0

Figure S7: Cyclic voltammogram of *fac*-[Re(ampy)(CO)$_3$(cbz$_2$phen)]$^+$ (A); *fac*-[Re(py)(CO)$_3$(cbz$_2$phen)]$^+$ (B); *fac*-[ReCl(CO)$_3$(cbz$_2$phen)] (C) in acetononitrile.
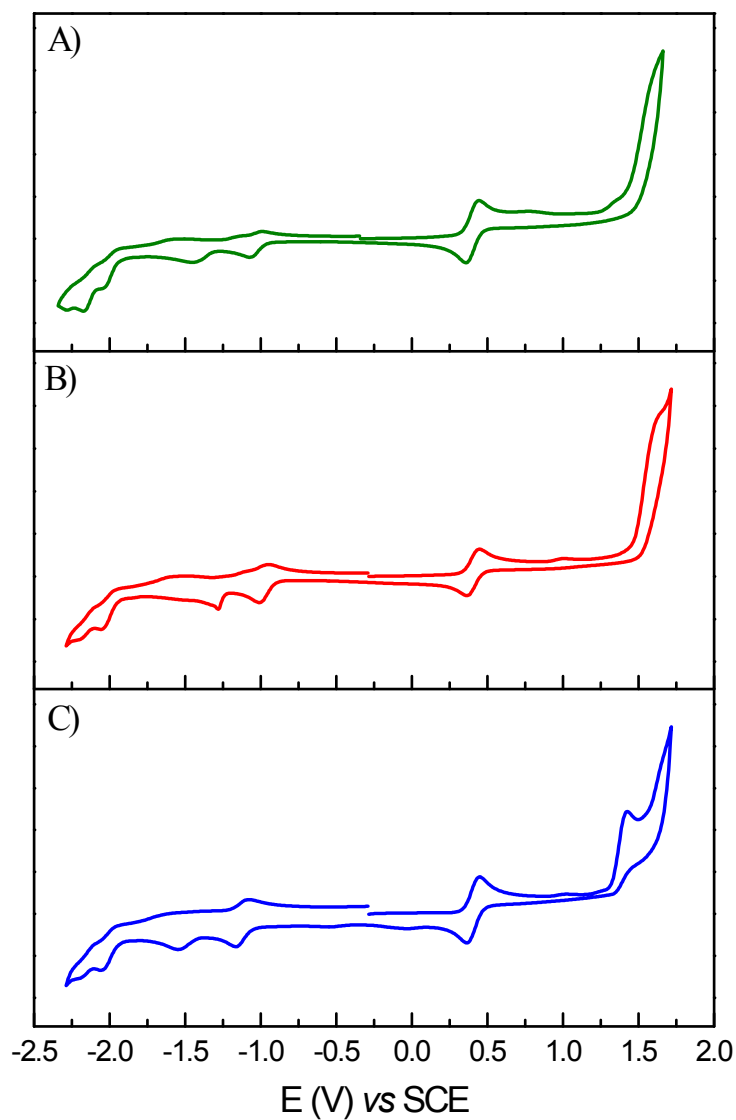
Figure S8: Experimental and theoretical spectra (A) and isosurfaces plots of frontier orbitals (B) of *fac*-[Re(py)(CO)$_3$(cbz$_2$phen)]$^+$ in acetonitrile.
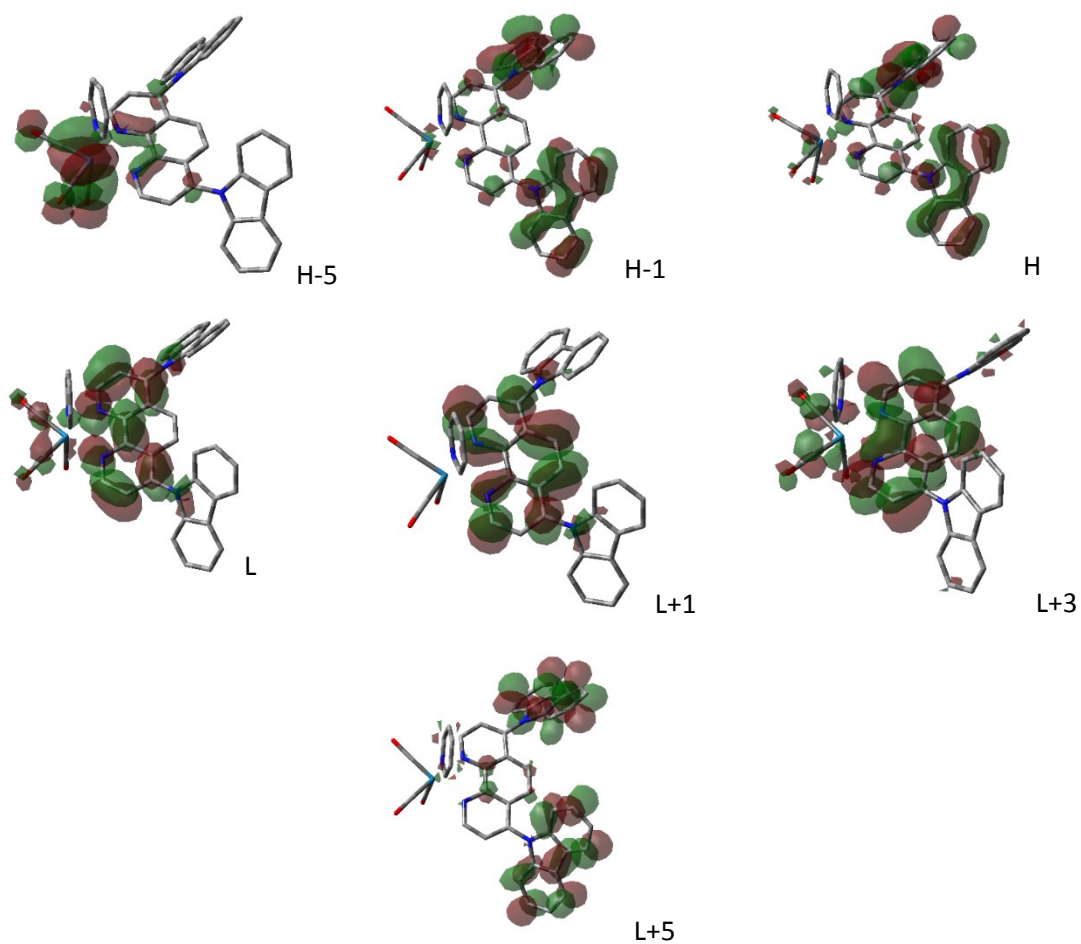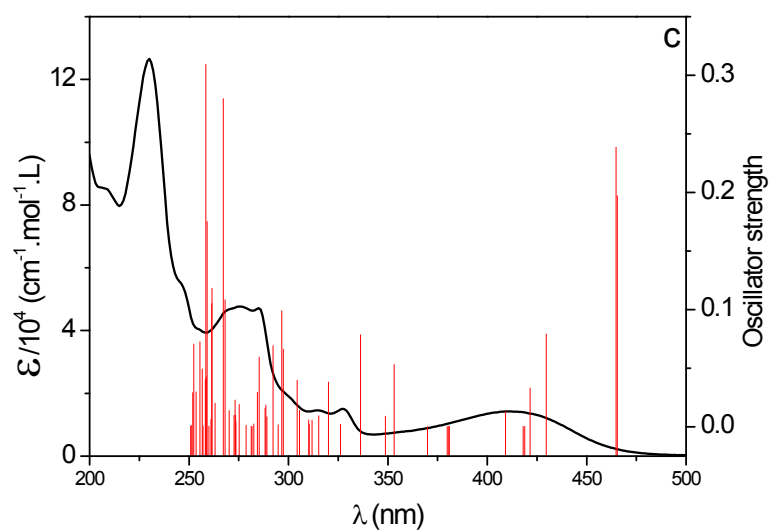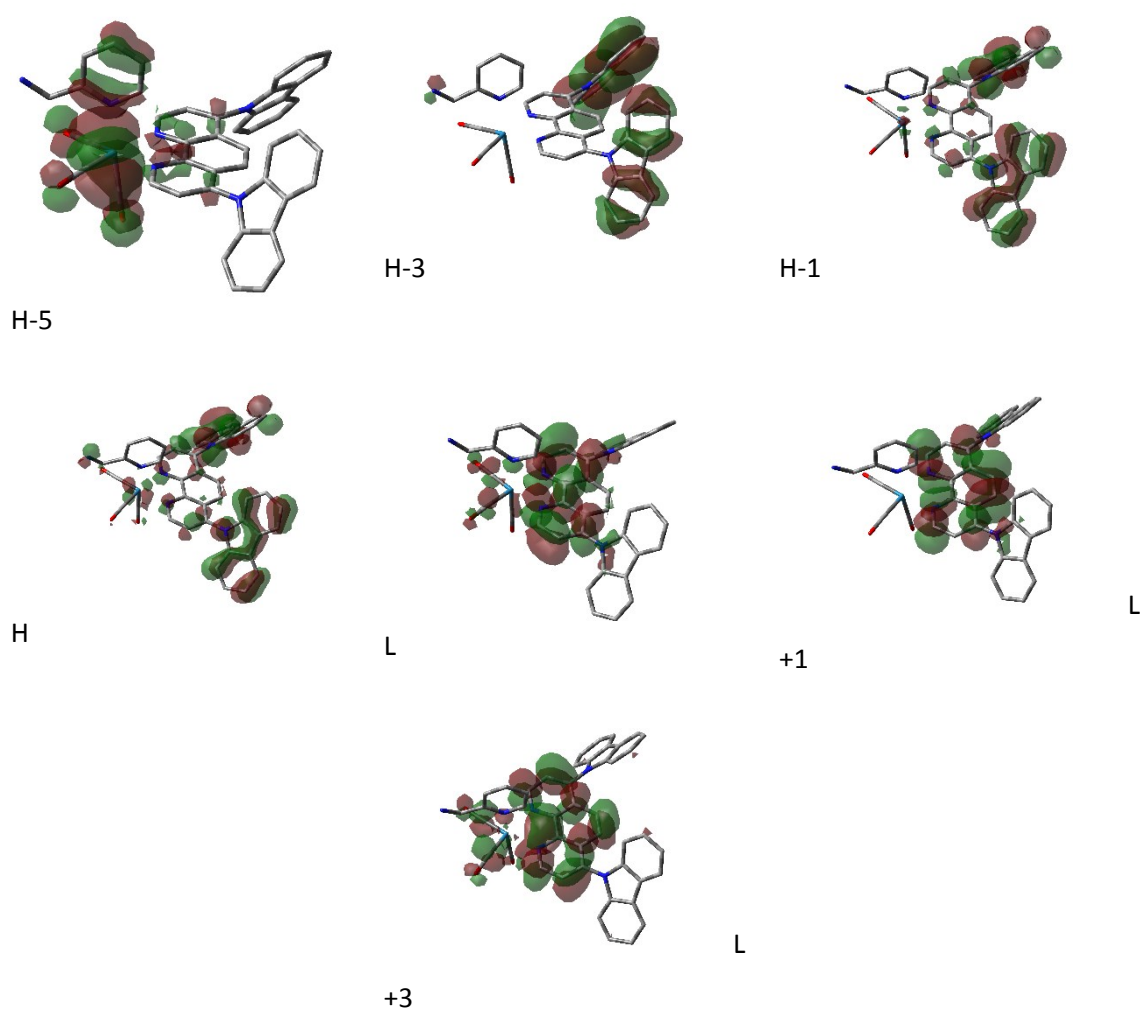
(A)

(B)

Figure S9: Experimental and theoretical spectra (A) and isosurfaces plots of frontier orbitals (B) of *fac*-[Re(ampy)(CO)$_3$(cbz$_2$phen)]$^+$ in acetonitrile.

(A)


(B)

H-5

H-3

H-1

H

L

+1

L

L

+3

Table S3: Theoretical spectral parameters of *fac*-[Re(L)(CO)$_3$(cbz$_2$phen)]$^+$ complexes in acetonitrile.

| X	Transition (contribution)	E (nm)	Oscillator strength	Mainly Character
py	H-1→L (78%)	455	0,2103	ILCT$_{cbz2phen}$
	H→L+1 (21)			ILCT$_{cbz2phen}$
	H→L (94%)	454	0,2596	ILCT$_{cbz2phen}$
	H-5 →L (97%)	366	0,0004	MLCT$_{Re→cbz2phen}$
	H-1→L+3 (58%)	293	0,173	ILCT$_{cbz2phen}$
	H→L+5 (11%)			IL$_{cbz2phen}$
ampy	H-1→L (72%)	466	0,1972	ILCT$_{cbz2phen}$
	H→L (13%)			ILCT$_{cbz2phen}$
	H→L+1 (13%)			ILCT$_{cbz2phen}$
	H-1→L (11%)	465	0,2386	ILCT$_{cbz2phen}$
	H→L (82%)			ILCT$_{cbz2phen}$
	H-5 → L (67%)	381	0,0004	MLCT$_{Re→cbz2phen}$
	H-5 → L (28%)	381	0,0005	MLCT$_{Re→cbz2phen}$
	H-3 → L+1 (56%)			ILCT$_{cbz2phen}$
	H-1→L+3 (83%)	297	0,0991	ILCT$_{cbz2phen}$

Figure S10: Isosurfaces plots of frontier orbitals of *fac*-[ReCl(CO)$_3$(phen)] and *fac*-[Re(py)(CO)$_3$(phen)]$^+$ in acetonitrile.

fac-[ReCl(CO)$_3$(phen)]   *fac*-[Re(py)(CO)$_3$(phen)]$^+$

LUMO+1

LUMO

HOMO

HOMO-1
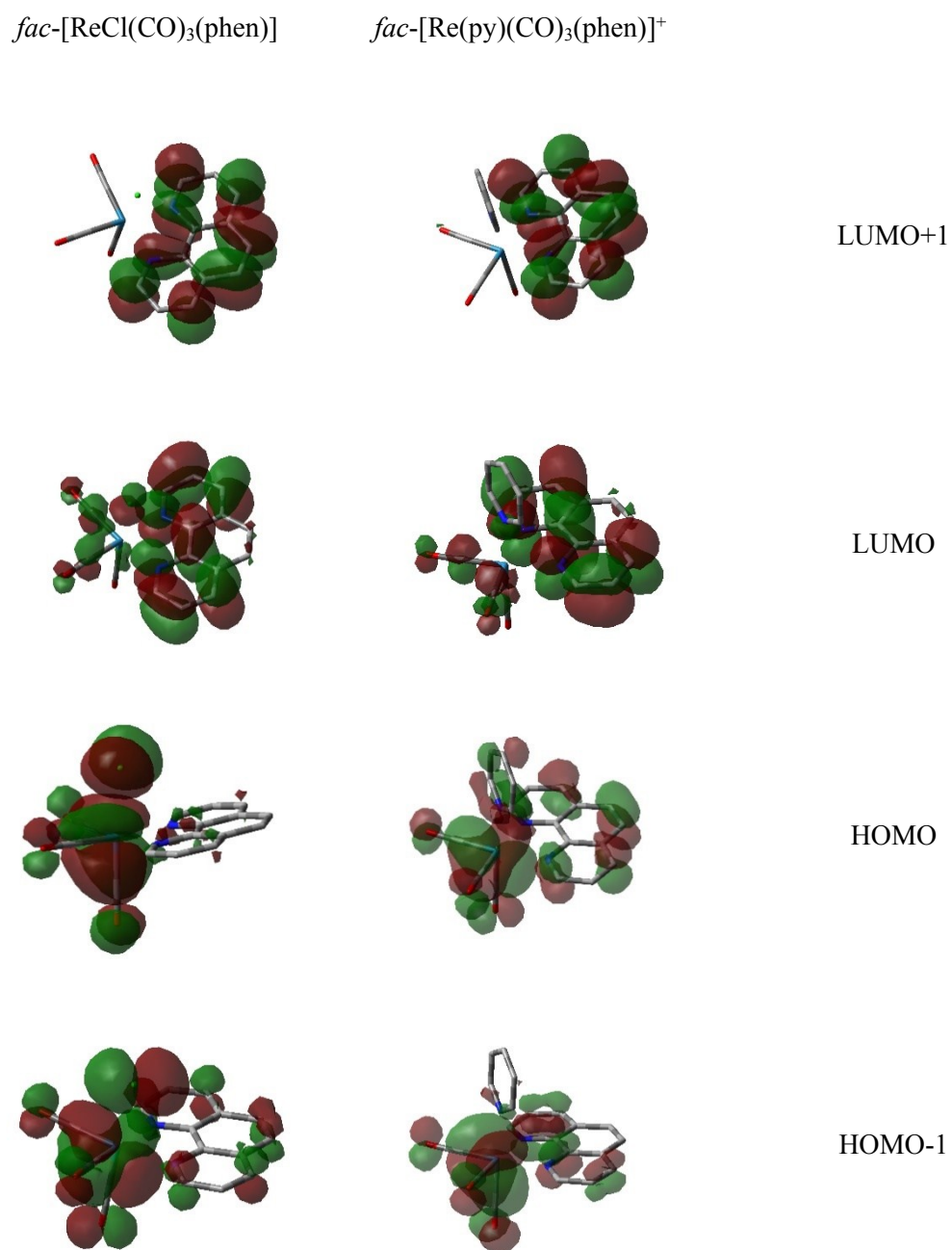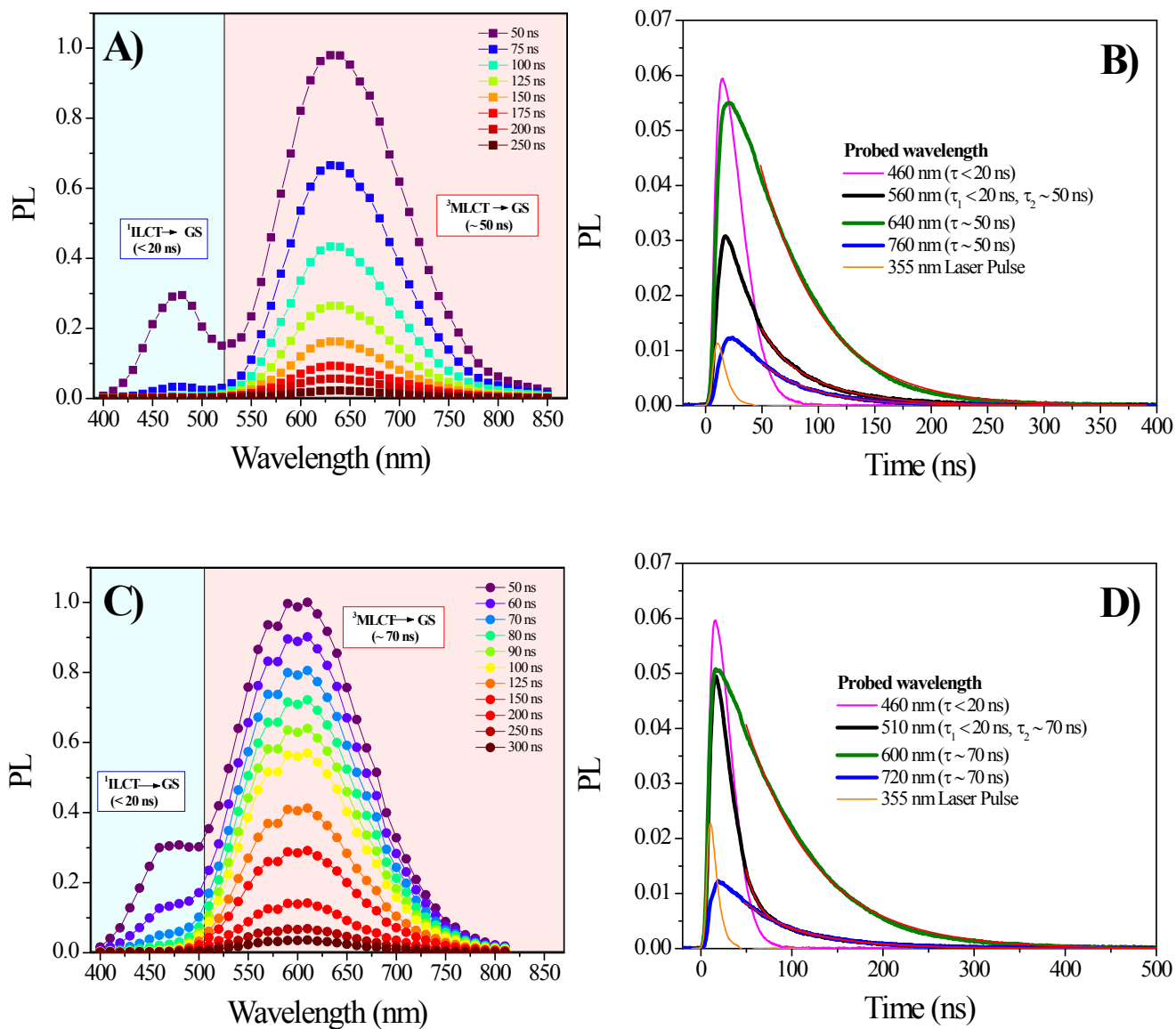
Figure S11: Changes in emission spectra of cbz$_2$phen in function of Zn^{2+} addition in acetonitrile. λ_{exc} = 355 nm.
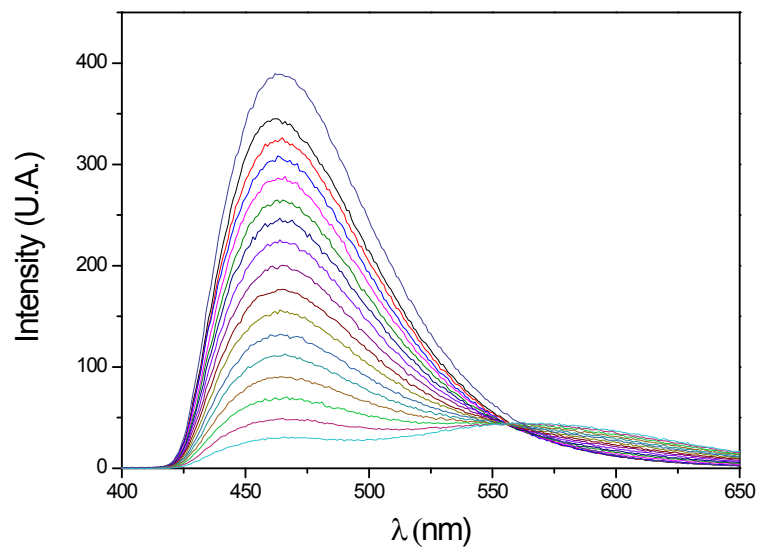
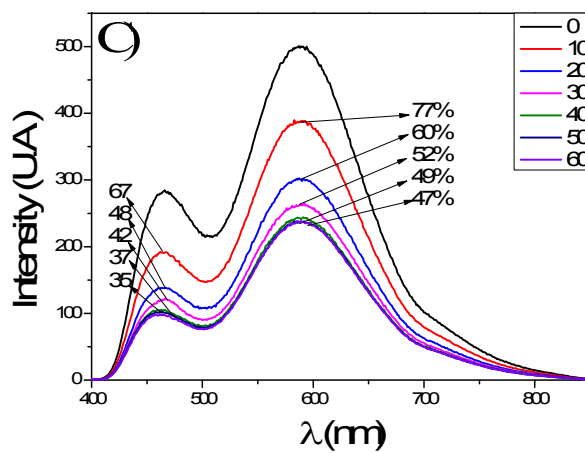**Figure S12**. Excitation Spectra of (A) *fac*-[ReCl(CO)$_3$(cbz$_2$phen)]; (B) *fac*-[Re(py)(CO)$_3$(cbz$_2$phen)]$^+$; (C) *fac*-[Re(ampy)(CO)$_3$(cbz$_2$phen)]$^+$, probed at two different wavelengths.
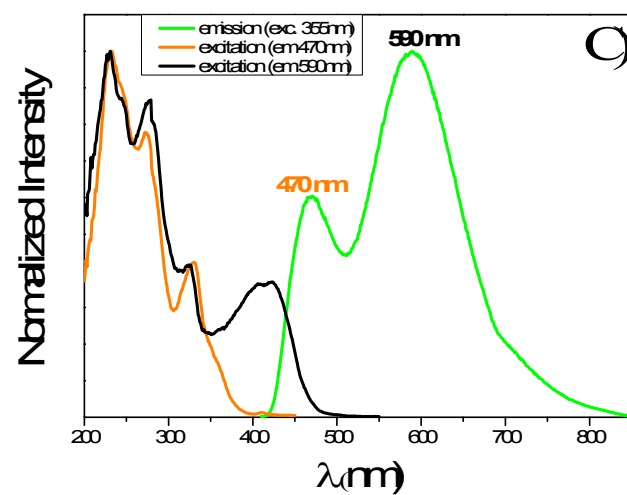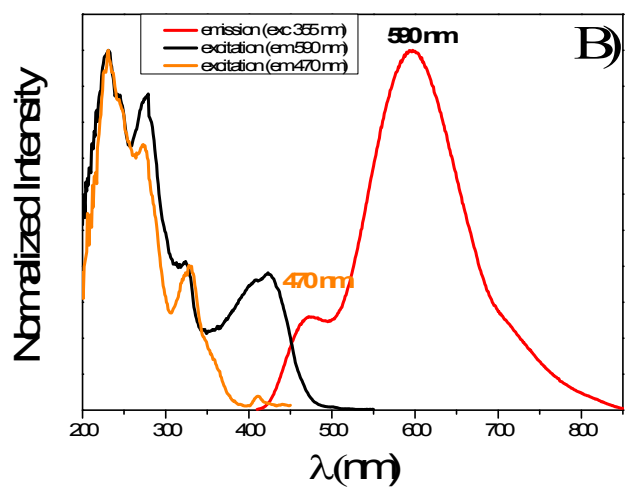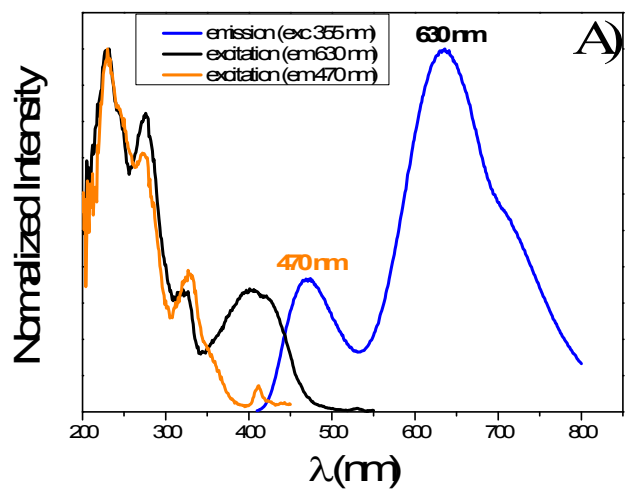
Figure S13: Time Resolved Photoluminescence Spectra of (A) *fac*-[ReCl(CO)$_3$(cbz$_2$phen)], (C) *fac*-[Re(py)(CO)$_3$(cbz$_2$phen)]$^+$ in acetonitrile solution, and their exponential fits (B) and (D) respectively.

Figure S14. Changes in emission spectra of (A) *fac*-[ReCl(CO)₃(cbz₂phen)]; (B) *fac*-[Re(py)(CO)₃(cbz₂phen)]⁺; (C) *fac*-[Re(ampy)(CO)₃(cbz₂phen)]⁺ in CH₃CN in function of O₂ addition. λ_{exc} = 355 nm. The legend inside each figure show the time, in second, of O₂ addition.
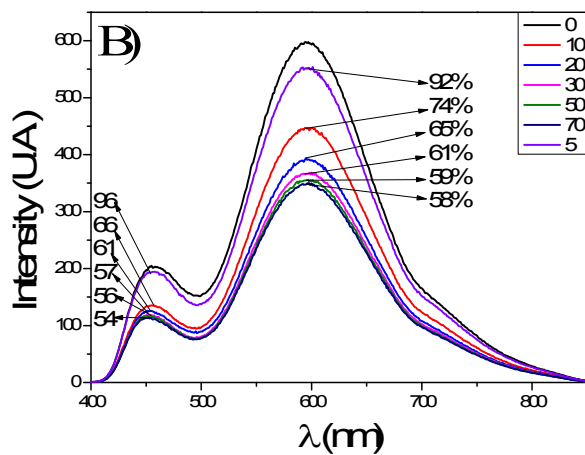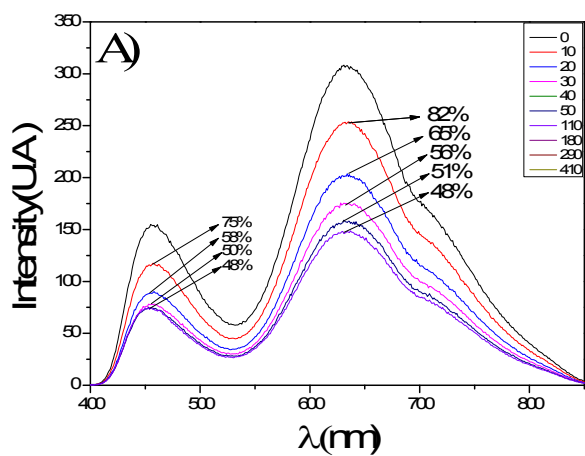
**Figure S15.** Changes in emission spectra of *fac*-[Re(py)(CO)$_3$(phen)]$^+$ in CH$_3$CN in function of O$_2$ addition. λ_{exc} = 355 nm. The legend inside the figure show the time of addition of O$_2$ in second.
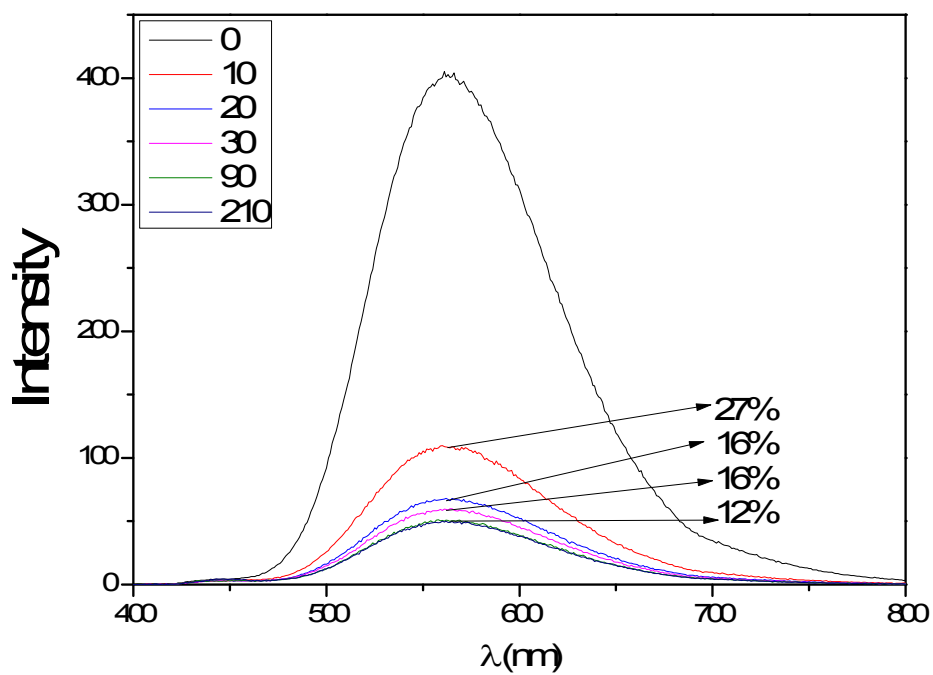
Figure S16: Time Resolved Photoluminescence Spectra of (A) *fac*-[ReCl(CO)$_3$(cbz$_2$phen)], (C) *fac*-[Re(py)(CO)$_3$(cbz$_2$phen)]$^+$, (E) *fac*-[Re(ampy)(CO)$_3$(cbz$_2$phen)]$^+$, in PMMA films, and their normalized spectra (B), (D) and (F) respectively.
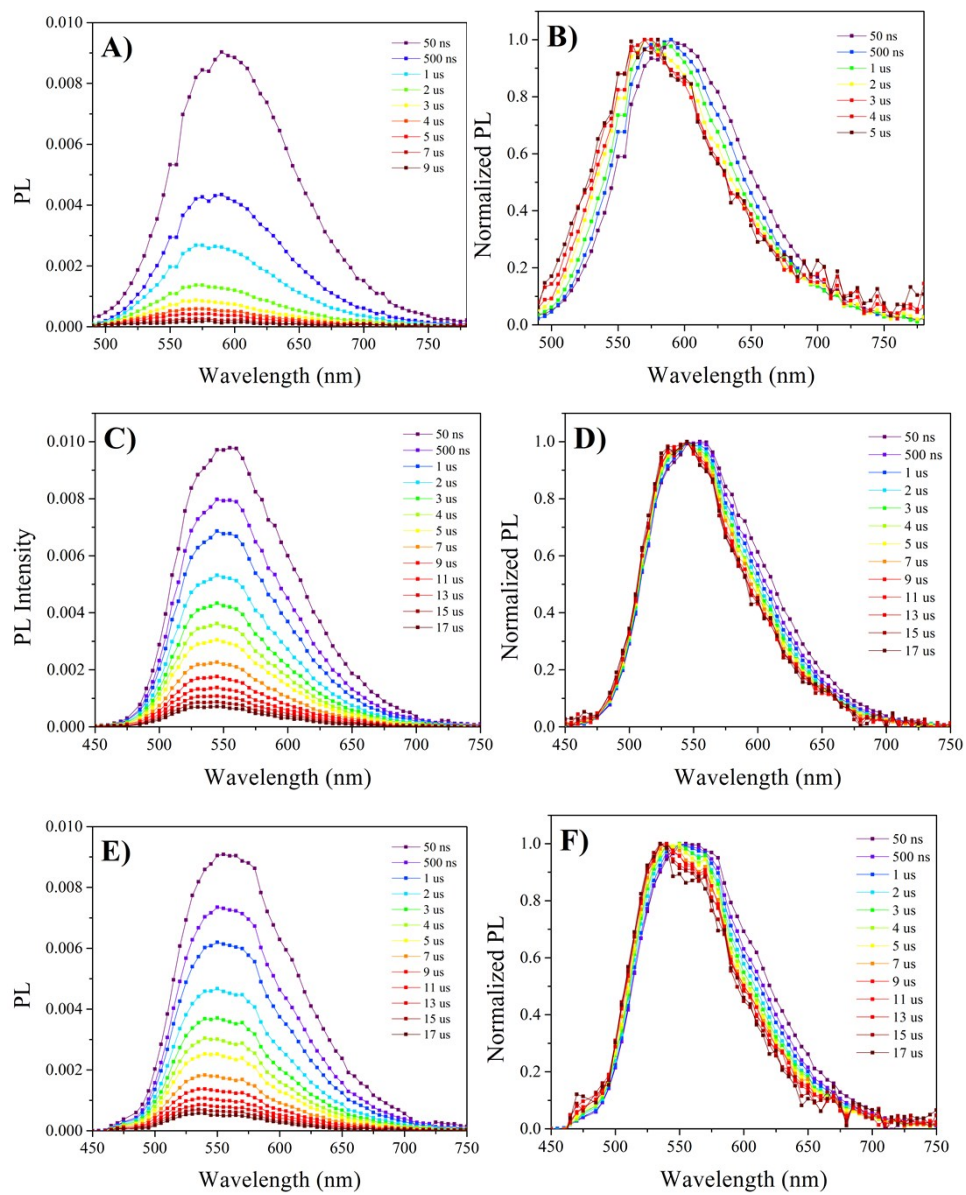
Figure S17: A) Experimental (dotted points) and simulated (solid lines) time resolved photoluminescence of (A) *fac*-[ReCl(CO)$_3$(cbz$_2$phen)] and (C) *fac*-[Re(py)(CO)$_3$(cbz$_2$phen)]$^+$ dispersed in PMMA film. The inset shows the obtained DAS Spectra containing the deconvoluted emitter states. (B) and (D) are the deconvoluted emission bands at different time delays for comparison. The inset diagram depicts the proposed dynamics for all compounds when in rigid PMMA medium.
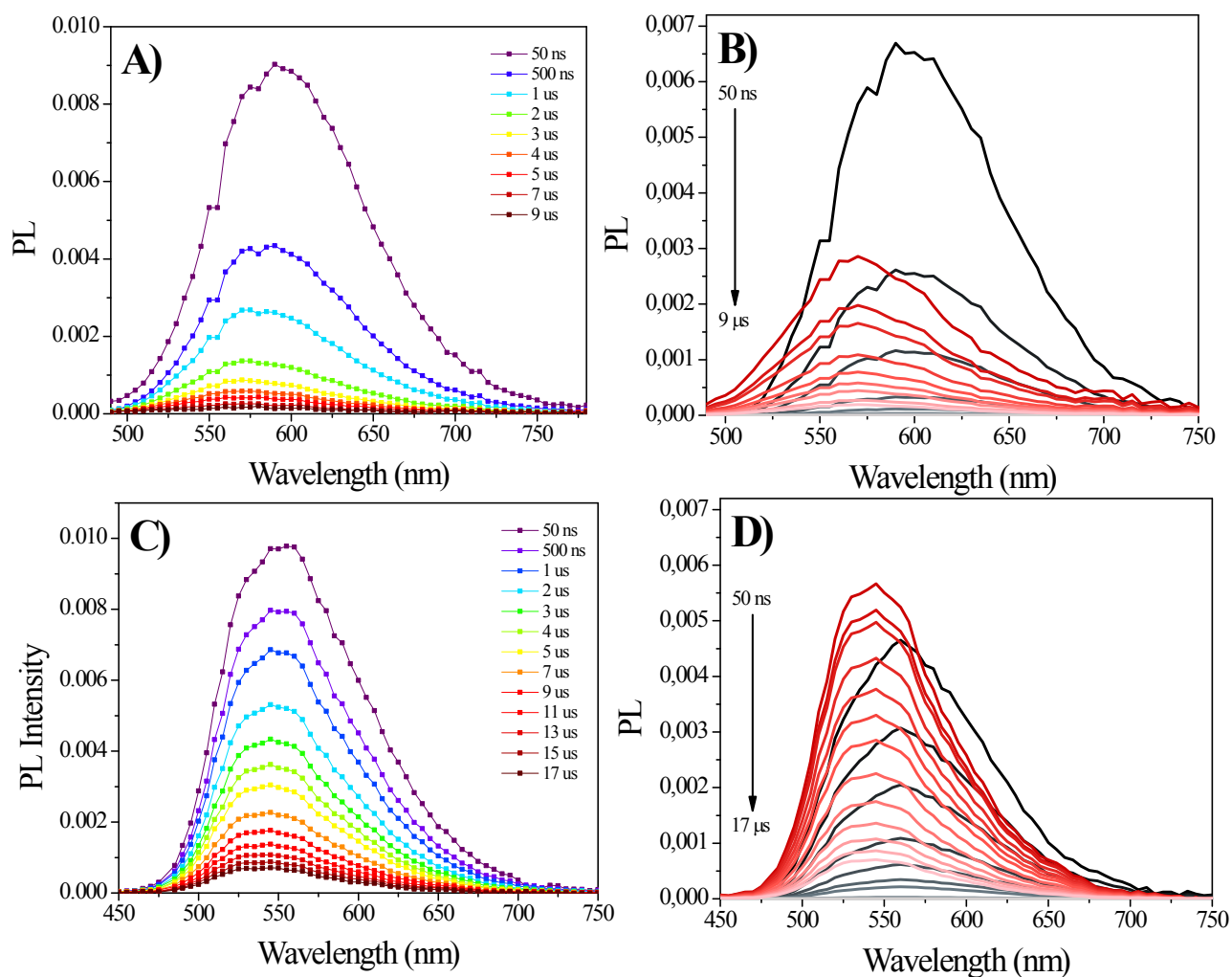
Figure S18: Bi-exponential fit at different wavelengths of the PL spectrum of (A) *fac*-[ReCl(CO)$_3$(cbz$_2$phen)]$^+$/PMMA, (B) *fac*-[Re(py)(CO)$_3$(cbz$_2$phen)]$^+$/PMMA and (C) *fac*-[Re(ampy)(CO)$_3$(phen)]$^+$/PMMA.